Key Points:
- Additional Saharan dust causes cooling and freshening of the North Atlantic amplifying Heinrich conditions
- Under a bistable AMOC state, enhanced Heinrich dust loading can cause an abrupt 20% reduction in AMOC without freshwater input
- Including both dust and freshwater forcing best matches the magnitude of eastern subtropical Atlantic cooling evident in proxy data

Supporting Information:
- Supporting Information S1

Correspondence to:
L. N. Murphy,
lmurphy@rsmas.miami.edu

The Role of African Dust in Atlantic Climate During Heinrich Events

L. N. Murphy[1] iD, M. Goes[2,3] iD, and A. C. Clement[1] iD

[1]Department of Atmospheric Science, Rosenstiel School of Marine and Atmospheric Science, University of Miami, Miami, FL, USA, [2]NOAA, Atlantic Oceanographic and Meteorological Laboratory, Miami, FL, USA, [3]CIMAS, University of Miami, Miami, FL, USA

Abstract Increased ice discharge in the North Atlantic is thought to cause a weakening, or collapse, of the Atlantic meridional overturning circulation (AMOC) during Heinrich events. Paleoclimate records indicate that these periods were marked by severe tropical aridity and dustiness. Although the driver of these events is still under debate, large freshwater input is necessary for climate models to simulate the magnitude, geographical extent, and abruptness of these events, indicating that they may be missing feedbacks. We hypothesize that the dust-climate feedback is one such feedback that has not been previously considered. Here we analyze the role of dust-climate feedbacks on the AMOC by parameterizing the dust radiative effects in an intermediate complexity model and consider uncertainties due to wind stress forcing and the magnitude of both atmospheric dust loading and freshwater hosing. We simulate both stable and unstable AMOC regimes by changing the prescribed wind stress forcing. In the unstable regime, additional dust loading during Heinrich events cools and freshens the North Atlantic and abruptly reduces the AMOC by 20% relative to a control simulation. In the stable regime, however, additional dust forcing alone does not alter the AMOC strength. Including both freshwater and dust forcing results in a cooling of the subtropical North Atlantic more comparable to proxy records than with freshwater forcing alone. We conclude that dust-climate feedbacks may provide amplification to Heinrich cooling by further weakening AMOC and increasing North Atlantic sea ice coverage.

1. Introduction

Proxy-based reconstructions from the most recent Heinrich stadial (HS1, ~17.5 ka) show that the Atlantic meridional overturning circulation (AMOC) was almost completely shutdown (McManus et al., 2004). In addition, the northern hemisphere tropics became drier (Peterson et al., 2000; Peterson & Haug, 2006; Stager et al., 2011; Wang et al., 2001), while the southern hemisphere tropics became wetter (Schefuß et al., 2005, 2011; Wang et al., 2004, 2006). Proxy records show strong concurrent cooling in the middle-to-high latitude North Atlantic (McManus et al., 2004), Iberian margin (Bard et al., 2000; Voelker et al., 2009), and in the subtropical central (Sachs & Lehman, 1999) and western Atlantic (Arienzo et al., 2015) during Heinrich stadials. To date climate model simulations of Heinrich events have been unable to replicate the broad geographic range of drying evident in paleoproxy data (Baker et al., 2001; Stager et al., 2011), and they impose large, and potentially unrealistic, amounts of freshwater input to significantly alter the AMOC (Calov et al., 2002; Kageyama et al., 2010; Roche et al., 2014; Zhang & Delworth, 2005). This suggests that models may be missing feedbacks necessary to trigger these events (Clement & Peterson, 2008). Recently, it was proposed that iceberg discharge may not be a cause of these events, but rather a consequence of ocean cooling (Barker et al., 2015).

Modern observations indicate that at times when the North Atlantic is anomalously cold, the tropical rainbelt shifts south, causing drying in the Sahel (Folland, Palmer, & Parker, 1986; Street-Perrott & Perrott, 1990; Wang et al., 2012). Tropical records from sediment cores in the eastern Atlantic show considerable variations in aridity and dust fluxes associated with cold periods in the North Atlantic (Jullien et al., 2007; Mulitza et al., 2008; McGee et al., 2013; Niedermeyer et al., 2009; Tjallingii et al., 2008). McGee et al. (2013) estimated that HS1 dust fluxes were a factor of ~2.6 higher than the late Holocene dust flux, while the Last Glacial Maximum (LGM) was only slightly dustier than the late Holocene. Increases in dust emissions further cool the North Atlantic by scattering solar radiation, thus leading to a positive feedback (Evan et al., 2011; Wang et al., 2012). Solar attenuation by dust aerosols not only cools SSTs but can also change the depth of the ocean mixed layer (Lau & Kim, 2007; Martinez Avellaneda et al., 2010). Moreover, Serra, Avellaneda, and Stammer (2014)

found that the propagation of dust-induced buoyancy anomalies caused small but statistically significant changes in AMOC in the 20th century. Climate simulations fall silent on the role of dust and its climate feedbacks because few paleoclimate simulations include interactive dust modeling. Recent efforts are improving the gap in this knowledge. For example, dust feedbacks during a Heinrich event were shown to cool the tropical north Atlantic in a simulation using an atmospheric model coupled to a slab ocean model (Murphy et al., 2014). In that study, changes in surface winds (not precipitation or soil moisture changes) were the dominant factor for driving enhanced dust emissions. It is plausible that regional wind changes, rather than ocean circulation changes, may have driven the large increase in Saharan dust during past Heinrich events. In fact, recent studies using both observations (Evan et al., 2016; Wang et al., 2015) and climate model experiments (Ridley, Heald, & Prospero, 2014) show that modern Saharan dust variability is largely controlled by wind speed changes over dust source regions and not changes in Sahel rainfall. Given the extreme magnitude of dust loading during HS1, and the uncertainty regarding the trigger for Heinrich events (Barker et al., 2015), the impact of dust could have a significant impact on ocean circulation at that time. Here we parameterize dust radiative effects in an ocean model to demonstrate for the first time the impacts of HS1 dust loading on AMOC.

The abrupt climate events of the last glacial and deglacial periods have been tied to the stability of the AMOC, where abrupt changes in freshwater input can cause transitions in the AMOC between stable "on" and "off" states (Bryan, 1986; Manabe & Stouffer, 1988; Rahmstorf et al., 2005; Stommel, 1961). As the AMOC weakens, less salt is transported northward, resulting in a further reduction in AMOC. This salt advection feedback (Stommel, 1961) is necessary for the AMOC to exist in multiple states (Rahmstorf, 1996) and is measured by calculating the freshwater transport at the southern boundary of the Atlantic (De Vries & Weber, 2005; Dijkstra, 2007; Drijfhout, Weber, & Swaluw, 2011; Hawkins et al., 2011; Huisman, den Toom, & Dijkstra, 2010; Rahmstorf, 1996; Weber et al., 2007). A negative freshwater transport at the southern boundary indicates a net import of salt and a bistable AMOC regime, whereas a positive freshwater transport at the southern boundary indicates an AMOC regime with only one stable state (Rahmstorf, 1996). In this study, we explore the impact of different prescribed wind stress on the stability of AMOC and analyze the freshwater content anomalies in response to freshwater forcing and Heinrich dust forcing under the two different AMOC states.

2. Methods

We utilize the University of Victoria (UVic) Earth system model, which consists of a three-dimensional ocean general circulation model, a dynamic thermodynamic sea ice model, a simple one-layer energy-moisture balance model of the atmosphere, and land-surface and dynamic terrestrial vegetation components (Weaver et al., 2001). The atmosphere calculates surface heat and freshwater fluxes without flux correction. UVic version 2.9 includes a variable latitudinal atmospheric diffusion of heat, which results in a much better fit to high-latitude LGM temperature proxies (Fyke & Eby, 2012). The ocean model is based on the Geophysical Fluid Dynamics Laboratory Modular Ocean Model 2.2 (Pacanowski, 1995) with a global resolution of 1.8° (meridional) by 3.6° (zonal) and has 19 layers in the vertical. The ocean vertical diffusivity is parameterized using the Bryan and Lewis (1979) vertical distribution. The sea ice component incorporates an elastic-viscous-plastic rheology to represent sea ice dynamics and sea ice thermodynamics and thickness distribution (Bitz et al., 2001).

We apply a simple parameterization of the dust effects on both shortwave and longwave radiations in UVic, based on a Heinrich simulation performed with the slab-ocean model version of Community Climate System Model version 4 (CCSM4) that was coupled to an interactive dust model (Murphy et al., 2014). Unlike CCSM4, UVic is very computationally efficient, which allows us to run multiple simulations to examine the sensitivity of the AMOC to the strength of the prescribed wind-stress forcing (section 2.1), the amount of dust forcing (section 2.2), and the amount of freshwater forcing (section 2.3). Table 1 summarizes the experiments performed for this study. All simulations are forced with LGM boundary conditions, including orbital forcing, trace gases, and ice sheets, as defined by the Paleoclimate Modelling Intercomparison Project phase 3 (PMIP3; Braconnot et al., 2011), and are spun-up from a 3,000 year long control LGM run. After the spin-up period, the two control simulations and all forced simulations are integrated for 1,000 years. Outputs are saved each decade.

Table 1
The Name of the Experiment (Column 1), the Length of Each Model Simulation (Column 2), the Prescribed Background Climatological Winds (Column 3), the Dust Forcing (Column 4), and the Freshwater Forcing (Column 5)

Name	Length	Winds	Dust	Freshwater (FW)
UVic LGM control	3,000 year spin-up +1,000 years	UVic	None	None
CAM LGM control	3,000 year spin-up +1,000 years	CAM	None	None
UVic H1	1,000 years	UVic	H1.0 (−LGM)	None
UVic H1.5	1,000 years	UVic	H1.5 (−LGM)	None
UVic H2	1,000 years	UVic	H2.0 (−LGM)	None
CAM H1	1,000 years	CAM	H1.0 (−LGM)	None
CAM H2	1,000 years	CAM	H2.0 (−LGM)	None
UVic FW	1,000 years	UVic	None	(0.01, 0.02, 0.03, 0.04, 0.05) Sv
CAM FW	1,000 years	CAM	None	(0.1, 0.2, 0.3) Sv
UVic FW + H1	1,000 years	UVic	H1.0 (−LGM)	(0.01, 0.02, 0.03, 0.04, 0.05) Sv
CAM FW + H1	1,000 years	CAM	H1.0 (−LGM)	(0.1, 0.2, 0.3) Sv

2.1. Wind-Stress Forcing

UVic is forced with prescribed climatological winds from the National Centers for Environmental Research (NCEP; Kalnay et al., 1996) and uses a dynamical wind feedback scheme, in which winds are allowed to change using a geostrophic/diffusive approximation in response to sea level pressure anomalies (Fanning & Weaver, 1997; Weaver et al., 2001). To account for the uncertainty in the climate response to the wind forcing, we run simulations using (i) standard "UVic" winds, in which surface pressure anomalies are calculated from surface temperature differences between our LGM control simulation and a long present-day control simulation, and then added as a perturbation to the prescribed mean wind/wind stress fields and (ii) "CAM" winds, in which the anomalous sea level pressures that are first subject to the UVic dynamical wind feedback are from differences between 100 year climatologies from the CCSM4 Last Glacial Maximum (LGM) and preindustrial (PI) simulations. The CCSM4 LGM and PI runs were part of the Paleoclimate Modelling Intercomparison Project phase 3 (PMIP3) and Coupled Model Intercomparison Project phase 5 (CMIP5) (Brady et al., 2013; Otto-Bliesner & Brady, 2010). After the spin-up, the resulting "CAM" wind climatology and mean surface temperature are used with the free wind feedback. Using this method, which is described in Goes, Wainer, and Signorelli (2014), avoids problems related to the different continental boundaries in the two models.

2.2. Dust Forcing

Anomalous dust aerosol optical depth (with respect to the LGM) from idealized Heinrich simulations in CCSM4 (Murphy et al., 2014) is used to parameterize the dust loading in UVic (Figure S1 in the supporting information). Dust both absorbs and scatters incoming solar radiation and outgoing planetary radiation, thereby modifying the radiative balance of the atmosphere. CCSM4 is used to quantify the effect of dust on the energetic balance of the atmosphere. The dust radiative forcing is calculated as the difference between the radiative forcing in a simulation that includes all aerosol species and a simulation including all aerosols except dust. The horizontal maps of shortwave and longwave dust radiation per unit optical depth of total LGM dust loading (not the HS1 anomalous dust loading) are used to tune UVic.

Previous studies have introduced the dust radiative effect in UVic by prescribing, at the top of the atmosphere, the shortwave and outgoing longwave anomalies simulated in a dust climate model (Schmittner et al., 2011). Here we follow a different approach, where we parameterize the effect of dust in UVic as a spatially resolved anomalous surface albedo forcing. The effect of dust on radiation in UVic is simulated as follows. The shortwave fluxes due to dust are parameterized as a perturbation of the local surface albedo (α_s):

$$\Delta\alpha_s = H\beta_s\tau(1 - \alpha_s)^2 \cos(Z_{eff}), \tag{1}$$

which is dependent on an upward scattering parameter (β_s), the aerosol optical depth (τ), the surface albedo (α_s), and the diurnally averaged effective solar zenith angle (cos (Z_{eff})). Here τ is the anomalous Heinrich (Heinrich-LGM) dust aerosol optical depth from CCSM4 in the tropical North Atlantic (100°W–30°E, 0°–30°N). We apply scaling factors on the dust shortwave effect to parameterize the dust longwave

radiation effects (i.e., top of the atmosphere outgoing (outlwr) and net surface (uplwr) longwave fluxes). Therefore:

$$\text{outlwr} = \text{outlwr}^* \; \max(0, (1.0 - \beta_O{}^* \, \Delta\alpha_s))), \tag{2a}$$

and

$$\text{uplwr} = \text{uplwr}^* \; \max(0, (1.0 - \beta_L{}^* \, \Delta\alpha_s)). \tag{2b}$$

The scattering parameter beta and the scaling parameters β_O and β_L are calibrated to best match the simulated radiative forcing response in CCSM4, accounting for the effects of dust on the absorption and reemission of terrestrial radiation. For this, we perform several 1 year long sensitivity runs changing these three parameter values and compare their output with CCSM4. The choice of these short sensitivity runs is to avoid measurable changes in ocean circulation, and the parameter calibration is performed for each parameter separately, first for shortwave (β_s), using a range of $\beta_s = 0.20$ to 0.27, and then for surface upwelling longwave ($\beta_L = 0.8$ to 1.7) and top of atmosphere outgoing longwave ($\beta_O = 0.1, 0.2$). The optimal parameters that give the best match between the CCSM4 and UVic dust radiative response are $\beta s = 0.23$, $\beta_O = 0.1$, and $\beta_L = 1.4$. The net dust radiative forcing due to LGM dust loading is shown in Figure S1 for the CCSM4 simulation (top) and in the tuned UVic simulation (bottom). The CCSM4 LGM dust optical depth that was used to tune UVic is overlaid as black contours in Figure S1. Over the North Atlantic dust belt (0°–30°N, 60°W–20°W), the reduction in net radiative forcing at the surface shows excellent agreement between both models with an average annual value of -2.20 W m^{-2} in CCSM4 and -2.22 W m^{-2} in UVic.

To investigate the sensitivity of the model to the dust, we define parameter H in equation (1) as the strength of the dust forcing. Parameter H can assume different values. We set $H = 1, 1.5$, and 2, where $H = 1$ represents the magnitude of anomalous dust optical depth forcing during the last Heinrich stadial (H1) (with respect to LGM) as simulated in CCSM4 (Figure 4; black contours), $H = 1.5$ is 1.5 times the anomalous dust optical depth, and $H = 2$ is 2 times the anomalous dust optical depth. The impact of increased Heinrich dust loading on top of the glacial (LGM) background state is defined as the difference between our anomalous dust forcing simulations (H1, H1.5, and H2) and the control (no dust).

2.3. Freshwater Forcing

We run additional simulations with various magnitudes of imposed freshwater forcing in the North Atlantic. Freshwater forcing is simulated as a virtual salt flux applied between 45°N and 65°N in the North Atlantic, which is approximately the latitudes of glacial ice debris referred as the Ruddiman belt (Ruddiman, 1977). We perform five experiments using a range of 0.01 to 0.05 Sv of FW forcing under UVic-wind forcing and three experiments using a range of 0.1 to 0.3 Sv of FW under CAM-wind forcing in the same region. The different amounts of freshwater forcing are chosen to allow a complete AMOC collapse under both prescribed UVic- and CAM-winds, given their differences in the strength and stability of the AMOC (described in section 3.2). Freshwater forcing is imposed for 200 years and is then turned off, which is within the range of duration of previous Heinrich climate model simulations (Kageyama et al., 2010; Roche et al., 2014). The cumulative amount of FW added to the North Atlantic ranges from 6×10^4 km^3 (FW = 0.01) to 3×10^5 km^3 (FW = 0.05) in the UVic-wind simulations, which is much smaller than the cumulative amount of FW added to the CAM-wind simulations (between 6×10^5 and 2×10^6 km^3). Each simulation is then run for an additional 800 years with no freshwater forcing to analyze the ability of AMOC to recover at the termination of H1. As in Kageyama et al. (2010) we do not apply a compensating salt flux. Stocker et al. (2007) showed that this compensation can cause unintended effects on Southern Hemisphere temperatures. The values of FW forcing under prescribed CAM-wind forcing are within the uncertainty range calculated in Roche et al. (2014).

2.4. Freshwater Budget

The Atlantic freshwater budget consists of the balance between the transport of freshwater by the ocean circulation and the water loss due to net evaporation. Thus, the net freshwater content anomaly (FWCA) (Wu & Wood, 2008) of the Atlantic basin (integrated from 34°S to the Bering Strait) is equal to the sum of the ocean freshwater transport, the surface freshwater flux, and a residual:

$$\text{FWCA} = \frac{1}{S_0}\frac{\partial S'}{\partial t} = \text{Mov} + \text{Maz} + \text{NET} + \text{Res}, \tag{3}$$

where S_0 is the difference between a reference salinity and the ocean salinity ($S_0 - S$) with $S_0 = 34.76$ psu. The freshwater transport by the ocean is decomposed into its main components: Mov, which is the meridional
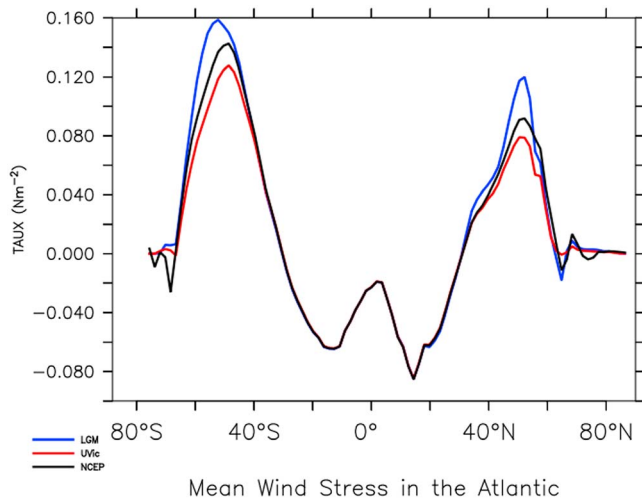
Figure 1. Annual mean zonal wind stress (Taux in N m^{-2}) averaged zonally over the Atlantic basin for NCEP present-day climatology (black), the LGM control with Uvic-winds (red), and the LGM control with CAM-winds (blue).

overturning component that is calculated using the total velocities, and Maz, which is the azimuthal component that encompasses the horizontal barotropic gyre circulation, and are defined as in Rahmstorf (1996) and Weijer et al. (1999). The net surface freshwater budget (NET) is the net surface precipitation, evaporation, runoff, ice melt, and brine rejection (Precip-Evap + Runoff + Ice) integrated from a southern boundary to the Bering Strait. Res is a residual term, which may arise from diffusion and mixing processes (Weber et al., 2007), nonstationary effects (Malanotte-Rizzoli et al., 2000), and computational errors along continental boundaries among others associated with the offline calculation of time-averaged fluxes. In UVic, the Bering Strait is closed; therefore, transport through the northern boundary is disregarded in (3). All ocean terms are integrated zonally and with depth across the Atlantic Ocean.

3. Results

3.1. The Influence of Wind Forcing on the Mean LGM State

The annual mean zonal wind stress of the control UVic-wind simulation shows a weakening of the westerlies relative to the NCEP climatology (Figure 1). CAM-winds, however, show stronger westerlies than NCEP. Although changes in the ITCZ are negligible using this approach, these changes in the mean wind state have strong implications for the AMOC strength and stability.

The LGM mean state for the simulation with UVic-winds is characterized by higher surface salinity in the tropics and lower surface salinity in the subpolar north Atlantic and at deep levels (1,000–3,000 m) (Figures 2a and 2b). The lower salinity at deep levels is due to a weaker southward advection by the NADW and a weaker and shallower AMOC (defined as the maximum value of the stream function in the north Atlantic) under UVic-winds (Figure 2e) compared to the CAM-winds control simulation (Figure 2f). This also makes the abyssal ocean less stratified and more homogenized under UVic-winds, a feature observed in previous model studies (Wainer et al., 2012). The UVic-wind control LGM simulation results in a much weaker AMOC (13 Sv, where 1 Sv = 10^6 m^3 s^{-1}) compared to the control present-day AMOC in UVic (~16 Sv) (Figure 2f). In the CAM-wind control LGM simulation, the AMOC strengthens to 22 Sv and expands northward (Figure 2e). The differences in AMOC strength agree with the large changes in the wind stress forcing in the subpolar North Atlantic and over the Southern Ocean (Figure 1). Models that participated in the Paleoclimate Model Intercomparison Project phase 3 (PMIP3) show that in the LGM, the presence of the Laurentide ice sheet causes a southward shift and strengthening of the westerlies, which leads to a more vigorous AMOC in these models (Brady et al., 2013; Muglia & Schmittner, 2015). In contrast, paleoclimatic proxy data suggest a weaker oceanic circulation during the LGM (McManus et al., 2004).

The location of North Atlantic ventilation also changes under the two wind regimes (Figures 2g and 2h). In the UVic-wind case, North Atlantic Deep Water (NADW) formation occurs just west of the British Isles, which is a common feature in coarse resolution ocean models (Cottet-Puinel et al., 2004). In the CAM-wind case, ventilation occurs just west of the British Isles and also in the Labrador Sea. In our control UVic-wind run, the sea ice edge extends further south and eastward than in the CAM-wind control simulation, and therefore, deep convection regions are displaced further east (black lines in Figures 2g and 2h). Current observational studies show that NADW occurs in the Nordic Seas and the Labrador Sea (Dickson & Brown, 1994), while proxy records suggest that NADW formed at more southern locations during the LGM than today (Labeyrie et al., 1992).

Studies have shown that advection of density anomalies from low to high latitudes in the North Atlantic can alter the AMOC (Vellinga & Wu, 2008), and changes in the freshwater content have been shown to play a dominant role on ocean circulation in the past (Schmittner et al., 2002). The mean surface freshwater budget of the Atlantic is very sensitive to the different climatological wind fields (Figure 3). In the control LGM mean climate, the freshwater content anomaly (FWCA) (equation (3)) can be neglected because transient effects are small. Thus, the surface freshwater flux (NET) is balanced by the ocean transports (Mov and Maz) plus a
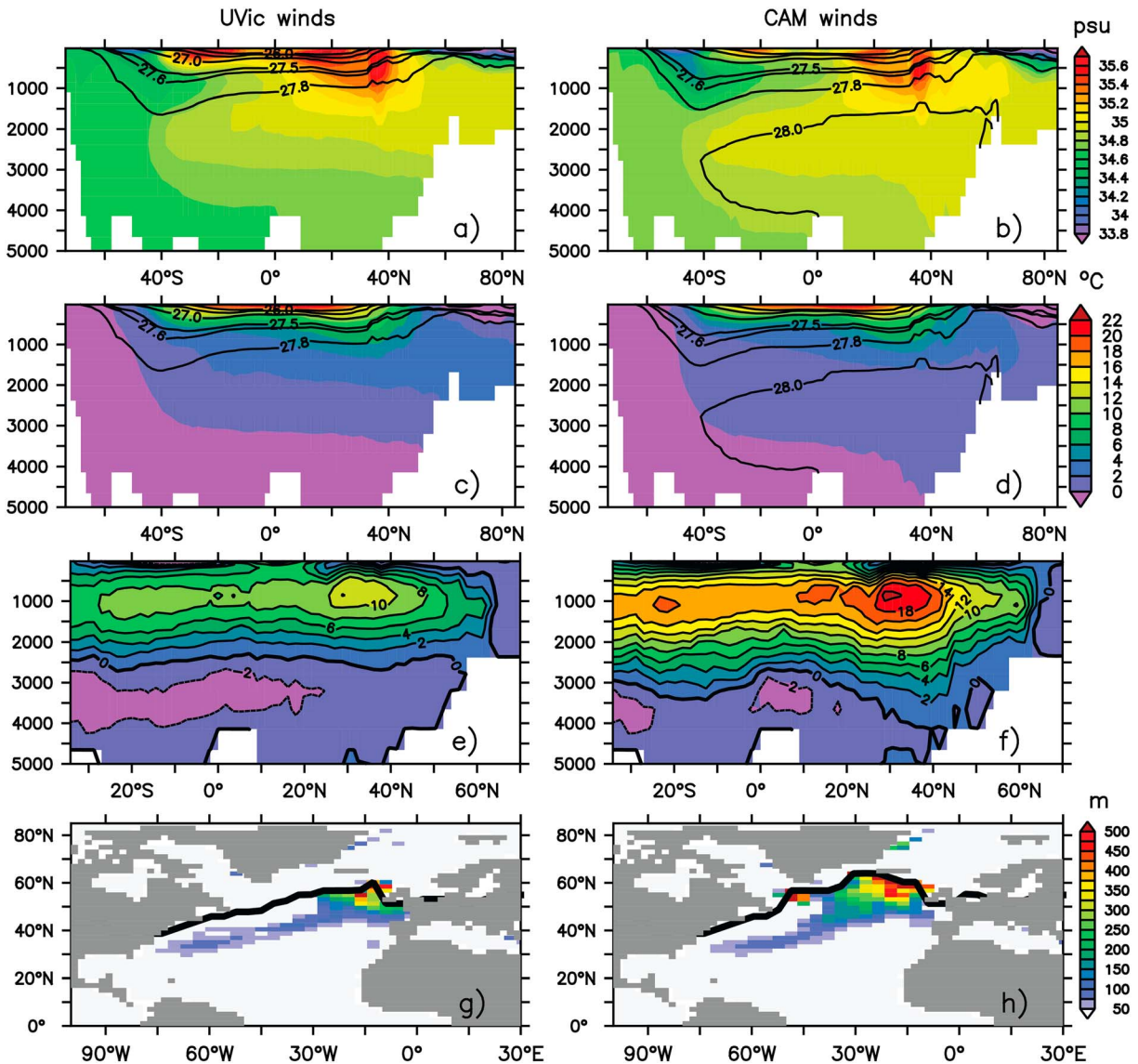
Figure 2. (a and b) Mean salinity, (c and d) temperature, and (e and f) AMOC stream function and (g and h) ventilation depth in the control LGM simulations using (left) UVic-winds and (right) CAM-winds. In Figures 2a–2d, the mean isopycnal depths are overlaid in black. In Figures 2g and 2h, the sea ice edge is overlaid in black.

residual. The net surface freshwater flux (NET) (blue lines in Figure 3) integrated north of 34°S is negative, with values of −250 mSv under CAM-winds and −150 mSv under UVic-winds, consistent with the idea that there is a net loss of freshwater at the surface to the atmosphere in the Atlantic Ocean. Under CAM-winds, the loss of freshwater at the surface in the Atlantic is compensated almost equally by the import of freshwater (positive) into the basin through the horizontal gyre (Maz) and overturning (Mov) circulations (~110 mSv for each component at 34.5°S). Conversely, under weaker westerlies (UVic-winds), the Mov across 34°S is negative and much weaker (−15 mSv); therefore, the loss of freshwater driven by surface freshwater fluxes (NET) and through oceanic overturning (Mov) is balanced almost solely by the transport of freshwater through the southern boundary via the gyre circulation (Maz = 150 mSv at 34°S). Interestingly, the mean transport by the gyre circulation at the southern boundary is fairly insensitive to changes in the mean overturning, so that Maz is similar under both wind forcing simulations. Intermediate complexity models have shown that a bistable regime occurs when the Mov is near or equal to zero (Weber et al., 2007). According to the sign of the Mov, the model can only simulate a stable "off" AMOC under UVic-wind forcing and is monostable (i.e., it only exists in one stable state) under CAM-wind forcing. This has large implications on the impact of Heinrich dust forcing on the AMOC, which is discussed in the next section.
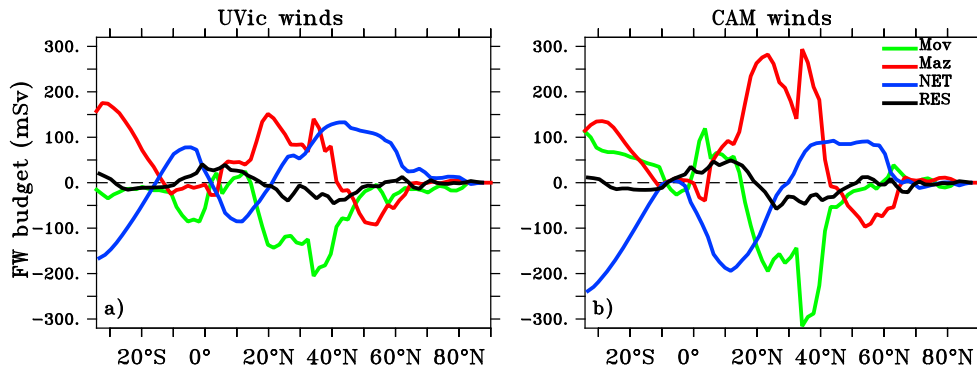
Figure 3. Mean freshwater budget in the Atlantic Ocean for the LGM control simulations under (a) UVic-winds and (b) CAM-winds. Mov: overturning component; Maz: gyre component; NET: surface forcing; RES: residual (NET-Mov-Maz).

3.2. Impact of Heinrich Dust on Climate

In this section, we test the sensitivity of the AMOC to H1 dust forcing alone in the absence of FW forcing. Figure 4 shows the anomalous (with respect to the LGM) H1 annual mean dust aerosol optical depth (DAOD) (contoured). The DAOD anomaly ranges from 0.02 to 0.18 over the Tropical North Atlantic. The enhanced dust loading reduces the net radiation at the surface from −0.5 to −6 W m^{-2} over the tropical North Atlantic (from 0° to 25°N) (shading Figure 4), with the largest reduction found closest to the African coast where the DAOD anomaly is largest. Albani et al. (2014) showed similar decreases in net surface radiation due to present-day dust loading over the North Atlantic (0–30°N).

The reduction of incoming radiation at the surface cools SSTs and weakens evaporation (Figures 5a and 5c). At the end of the first decade, the strongest cooling is located under the anomalous DAOD. Under H1 (H2) dust forcing the initial (averaged over the first decade) cooling in the Tropical North Atlantic is 0.17°C (0.32°C) under UVic-winds and 0.18°C (0.35°C) under CAM winds. In comparison, Evan et al. (2011) used an ocean general circulation model to estimate an anomalous cooling in the Tropical North Atlantic of up to 0.3°C between the five most dusty and least dusty years over the 20th century. Reduced surface freshwater fluxes (evaporation minus precipitation and river runoff) over the eastern subtropical North and South Atlantic result in a reduction in the near surface salinity (Figures 5b and 5d). The anomalously freshwater becomes trapped within the shallow subtropical cells, which connect the subtropics to the equatorial Atlantic (not shown), while the Caribbean Sea and western subtropical North Atlantic show increased salinity. The initial cooling and freshening due to the H1 dust forcing show highly similar magnitudes and spatial patterns regardless of the prescribed wind forcing.

Under CAM-wind stress forcing, H1 dust forcing results in no significant AMOC change relative to control (Figure 6b). In contrast, under UVic-wind stress forcing, H1 dust forcing results in an abrupt 20% (2.8 Sv) reduction in AMOC after roughly 600 years of model integration (Figure 6a). Sensitivity experiments with increased strength of the dust forcing (H1.5 and H2.0) show no impact on the magnitude of the AMOC changes, only impacts on the timing of the AMOC slowdown, with larger dust forcing resulting in a faster AMOC reduction (~200 years for H1.5 and ~60 years for H2.0 dust, compared to 410 years for H1.0 dust). A weaker AMOC in our UVic-wind control simulation results in less northward oceanic heat transport (OHT) compared to our CAM-wind control simulation (0.6 PW and 0.9 PW, respectively; black lines in Figures 6c and 6d). We compare the OHT in the UVic and CAM-wind control simulations to the simulations with H1 dust forcing at model year 500. The 20% reduction in AMOC under UVic-winds results in a nearly 0.1 PW reduction in OHT (Figure 6c, green line) compared to the control (Figure 6c, black line), while under prescribed CAM-winds H1 dust forcing alone does not change the magnitude of OHT (Figure 6d, green line). Eddy heat transport (dashed
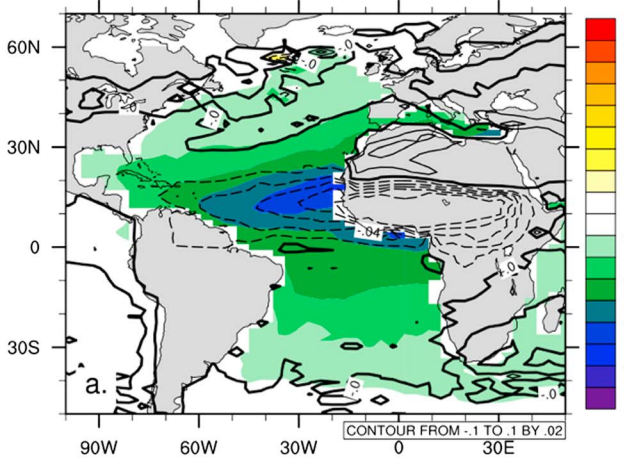
Figure 4. The anomalous (H1-control) dust aerosol optical depth (DAOD; contours) prescribed in UVic and the associated reduction in net surface radiation (shading) due to the anomalous DAOD calculated as the difference in net shortwave minus net longwave at the surface averaged over 1 year of simulation.
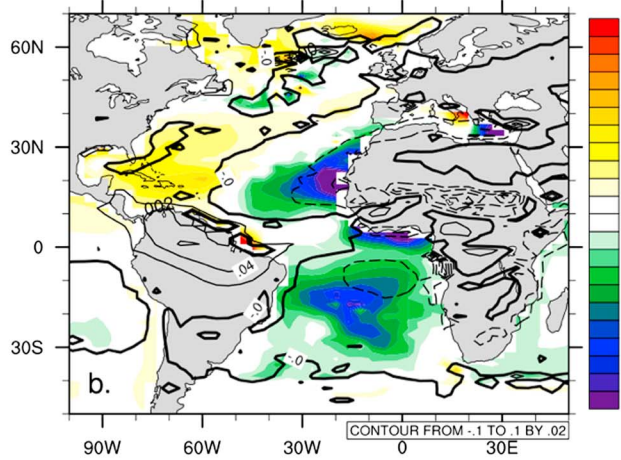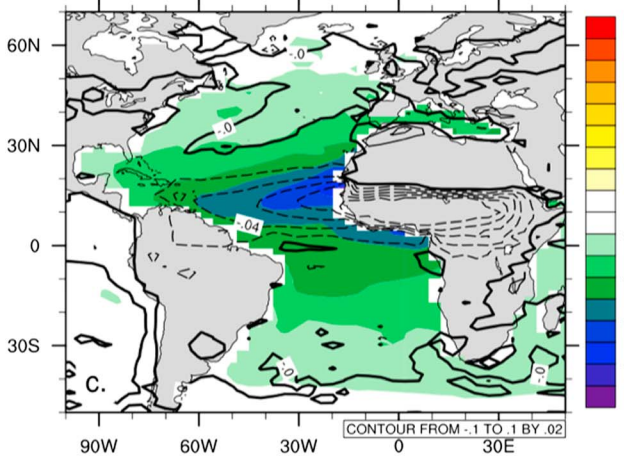
UVic-winds: H1 - LGM
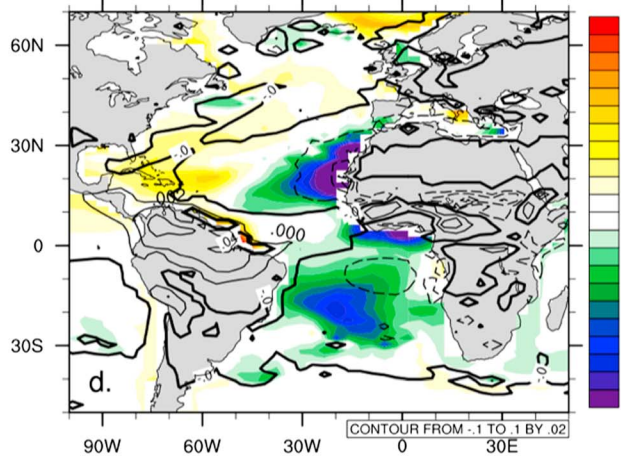
CAM-winds: H1 - LGM

Figure 5. H1-LGM anomalies for the (a and b) UVic wind experiments and (c and d) CAM-wind experiments of near-surface ocean potential temperature (shaded; °C) and evaporation (contours; mm d^{-1}) (Figures 5a and 5c) and H1-LGM anomalies of near-surface ocean salinity (shaded; psu) and surface freshwater flux (evaporation-precipitation-runoff; mm d^{-1}) anomalies (Figures 5b and 5d). All variables were averaged over the first decade (years 0–10).

black lines in Figures 6c and 6d), which are parameterized using the Gent and Mcwilliams (1990) scheme, show strong resemblance with the estimates from higher resolution models (Tréguier et al., 2012; Valdivieso et al., 2014) but remain unchanged in the anomalous dust simulations.

Initially, changes in the surface heat fluxes are confined to the subtropics where the H1 dust forcing is applied and are similar under both UVic and CAM-winds (Figures 7a and 7b). The decrease in shortwave radiation at the surface due to dust loading is partly balanced by enhanced latent heat flux and longwave radiation. In contrast, at the end of the simulations, differences in the surface heat flux arise between the CAM-wind and UVic-wind experiments due to changes in the AMOC. Less northward OHT in the UVic-wind simulations with H1 dust results in a large increase in the net total heat flux in the subpolar north Atlantic over the last century (Figure 7d). However, minimal changes occur in the CAM-wind simulations with H1 dust (Figure 7c). In the UVic-wind experiments, anomalous H1 dust leads to a cooling of up to −1.9°C in the last decade of model simulation, and the largest cooling is found in the high latitudes between 40 and 60°N (Figure 8a). In addition, the high latitude North Atlantic is fresher while the rest of the Atlantic is saltier (Figure 8b). A 10–40% increase in sea ice occurs in the North Atlantic, and sea ice extends further south (Figure 8d). The largest increase in sea ice is found just west of the British Isles where there is a concurrent decrease in
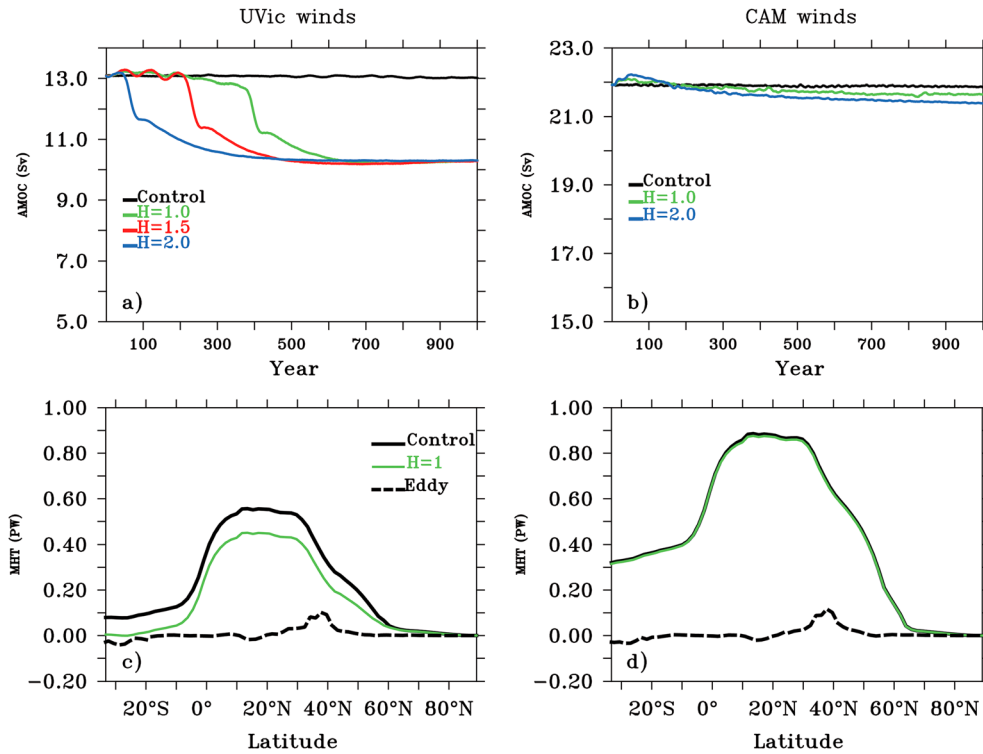
Figure 6. (a and b) AMOC strength for LGM control run (black) and for the dust experiments with dust forcing equal to $H = 1.0$ (blue), $H = 1.5$ (red), and $H = 2.0$ (green). (c and d) Atlantic meridional heat transport (MHT in PW) averaged over the last century (model years 900–1,000) for the LGM control run (black), H1 dust ($H = 1.0$; green), and for the eddy velocities only (dashed black). Results for the UVic-wind experiments are on the left (Figures 6a and 6c) and for the CAM-wind experiments are on the right (Figures 6b and 6d).
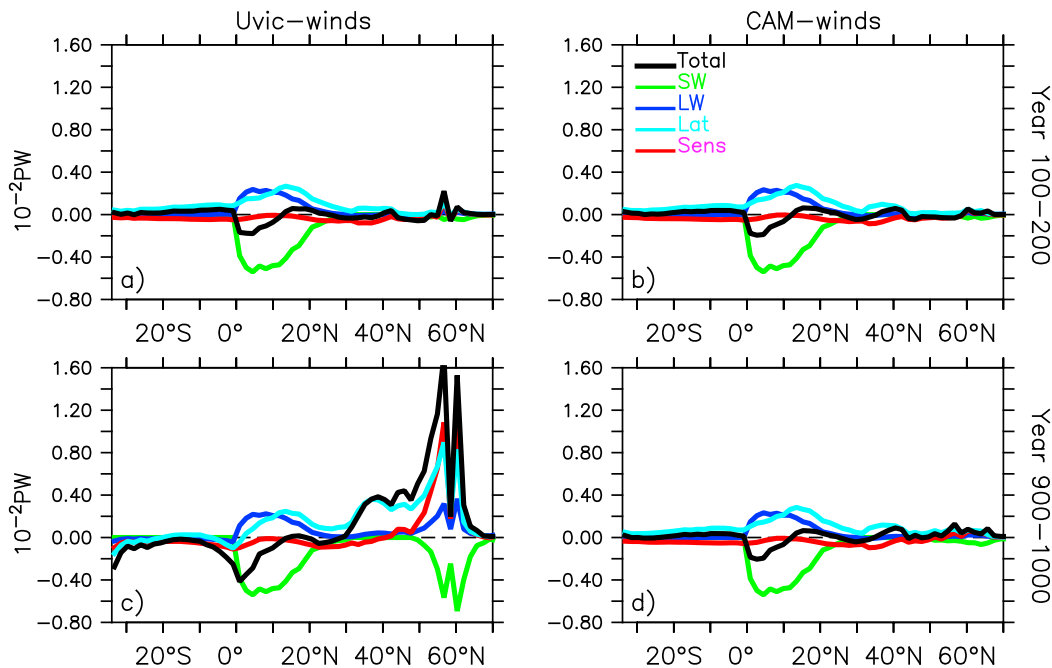
Figure 7. Shortwave (SW), longwave (LW), sensible (Sens), latent (Lat) and total heat flux components integrated at every grid point and zonally averaged over the (a and b) first century (model years 0–100) and the (c and d) last century (model years 900–1,000) for (left) UVic-winds and (right) CAM-winds. Fluxes are defined as positive downward and are given in units of 10^{-2} Petawatt (PW).
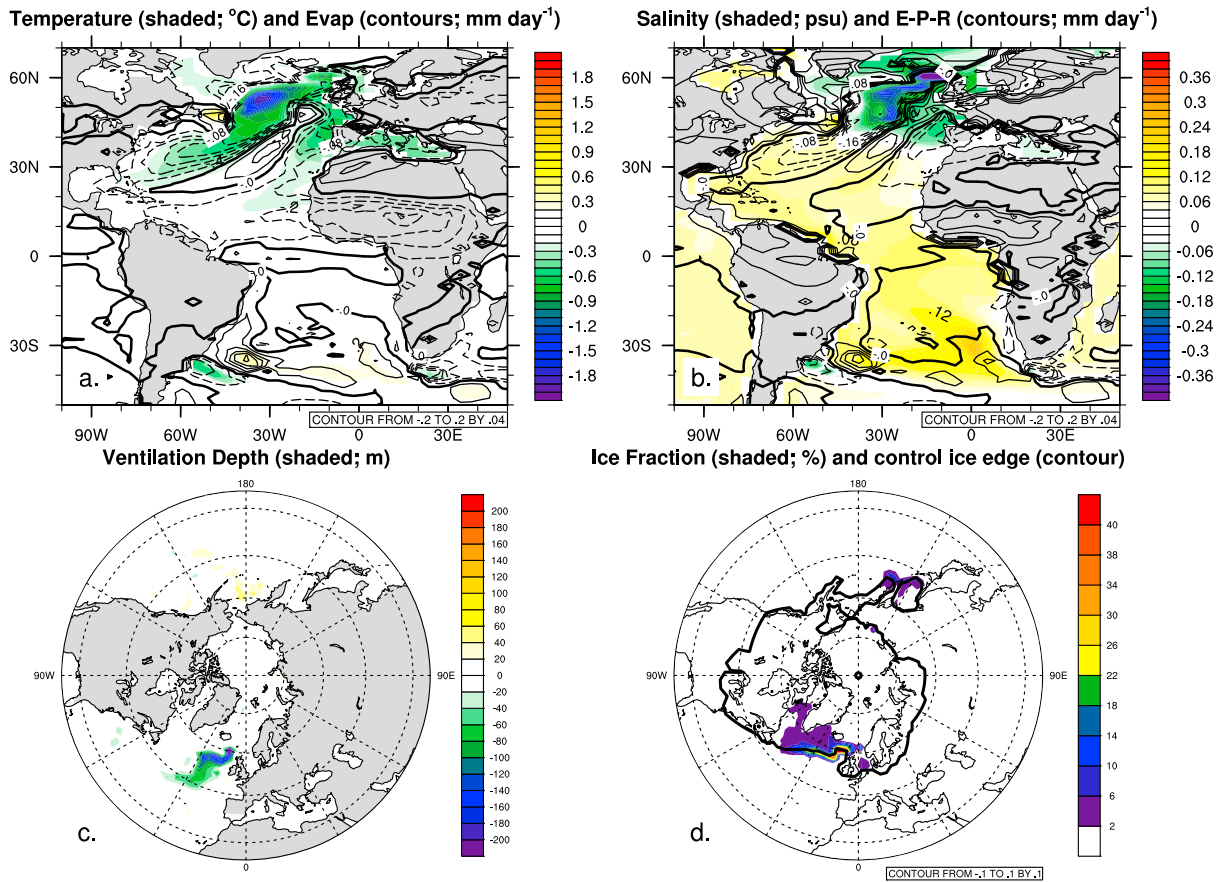
Figure 8. (a) UVic-wind H1-LGM anomalies of near-surface ocean potential temperature (shaded; °C) and evaporation (contours; mm d^{-1}), (b) near-surface ocean salinity (shaded; psu) and surface freshwater flux (evaporation-precipitation-runoff; mm d^{-1}), (c) ventilation depth (shaded; m), and (d) sea ice fraction (shaded; in %) with the ice edge in the control simulation overlaid with black contour line. All variables were averaged over the last decade (years 990–1,000).

ventilation depth (Figure 8c). The zonally averaged heat budget shows that the decrease in shortwave radiation, in part due to the expansion of sea ice, is compensated by an increase in turbulent heat fluxes and longwave radiation (defined as positive downward) (Figure 7c).

The sensitivity of AMOC response (Figures 6a and 6b) is likely driven by ocean circulation and ice feedbacks to the adjustment of the freshwater budget. To examine this assumption, we examine the impact of H1 dust forcing on the Atlantic freshwater budget. The changes in the freshwater content terms are calculated as the difference between the H1 dust and the control LGM simulations. We decompose the surface freshwater flux (NET) anomalies (H1-control) into its main components: precipitation (Precip), evaporation (Evap), river discharge (Runoff), the change in northern hemisphere sea ice volume (ice), and total (NET) (Figures 9a and 9b). In both simulations (Figures 9a and 9b), the cooling effect of dust reduces evaporation and is only partly compensated by the decrease in river runoff and precipitation, thus freshening the North Atlantic. Therefore, there is an initial increase in NET of about 2–3 mSv (Figures 9c and 9d). The enhanced NET causes an equal increase in the freshwater content (FWCA) by ~2–3 mSv before any changes in total oceanic freshwater transport (OcT; Figures 9c and 9d). In the CAM-wind simulation, OcT increases by ~3 mSv in the year 100, driven mostly by an increase in freshwater transport by the overturning circulation (Mov; ~6 mSv), and partially compensated by a reduction in freshwater transport by the gyre circulation (Maz; ~−3 mSv). This initial increase in Mov is a response to a small increase in the AMOC (Figure 6b), most likely due to the initial cooling of the North Atlantic basin. After year 100 in the CAM-wind simulation, Mov decreases and drives most of the anomalous OcT divergence later on. The anomalous divergence of oceanic freshwater transport compensates the increased NET in the end of the CAM-wind run (Figure 9d).
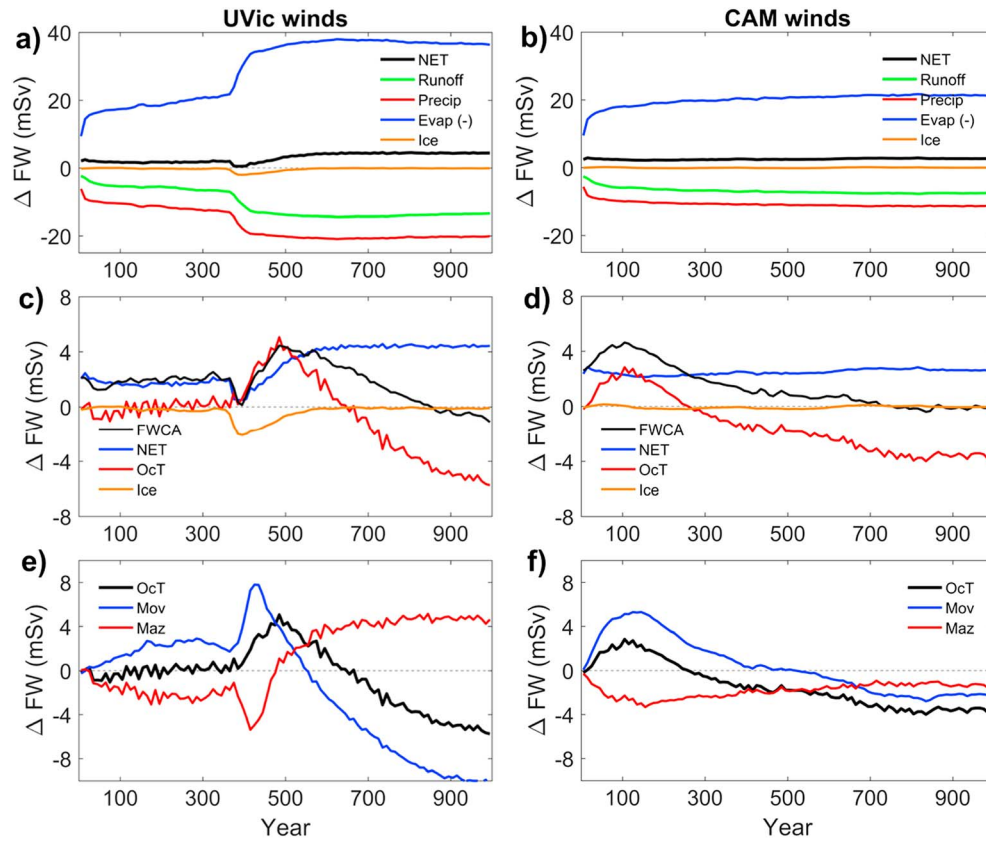
Figure 9. Time evolution of the Atlantic freshwater budget anomalies (H1-LGM control) integrated north of 32.5°S for the simulations using (left) UVic-winds and (right) CAM-winds. (a and b) The surface freshwater flux components: runoff (green), precipitation (red), evaporation (blue), ice (orange), and the combined net freshwater flux (black). Note that evaporation was multiplied by negative 1 to denote a negative freshwater anomaly. (c and d) the total freshwater content anomaly (FWCA), surface (blue), ocean (red), and ice (orange); (e and f) the ocean freshwater transport (OcT) and its Mov (blue) and Maz (red) contributions.

In the Uvic-wind simulation the scenario is more complex due to stronger sensitivity of ocean circulation to the heat and freshwater changes. The initial OcT changes are negligible because of a strong compensation between an increased Mov and a decreased Maz before model year 350 (Figure 9e). At approximately year 350, a sharp increase in the North Atlantic sea ice results in an abrupt reduction in NET and FWCA via brine rejection (Figure 9c), and an increased Mov of ~8 mSv, that is partially compensated by reduced Maz, which results in an oceanic freshwater convergence of ~4 mSv. There is an additional cooling and NET increase in the North Atlantic due to the impact of ice changes on the surface fluxes (Figure 7c). When the ice growth diminishes, the large-scale freshening dominates the OcT variability, and there is a strong decrease in the overturning circulation (Mov) reducing the oceanic import of freshwater into the basin. A final balance is then reestablished between the anomalous NET and OcT (Figure 9e). It is important to notice that the Mov and Maz anomalies given in Figure 10 are not strong enough to change their signs; therefore, Mov still exports freshwater in the Uvic-wind experiments and imports freshwater in the CAM-wind experiments.

We analyze the difference in surface freshwater flux changes under different amounts of dust loading in the UVic-wind experiments (H1, H1.5, and H2). The NET freshwater anomalies forced by dust north of 34°S after 1,000 years are 4 mSv (H1; Figure 9c), 5 mSv (H1.5), and 6 mSv (H2). The different amounts of surface freshwater flux trigger a faster FWCA response, which explains the time difference in triggering the AMOC slowdown between the experiments (Figure 6a). The total reduction in the strength of the AMOC (~20%) is insensitive to the different amounts of dust forcing in our simulations, even though the surface NET response is larger under stronger dust radiative forcing. As a balance between OcT and NET is expected to be reestablished at the end of all dust simulations, we conclude that it is not the velocity adjustment (v') but the salinity (S') distribution along 34.5°S that changes under different dust forcing.
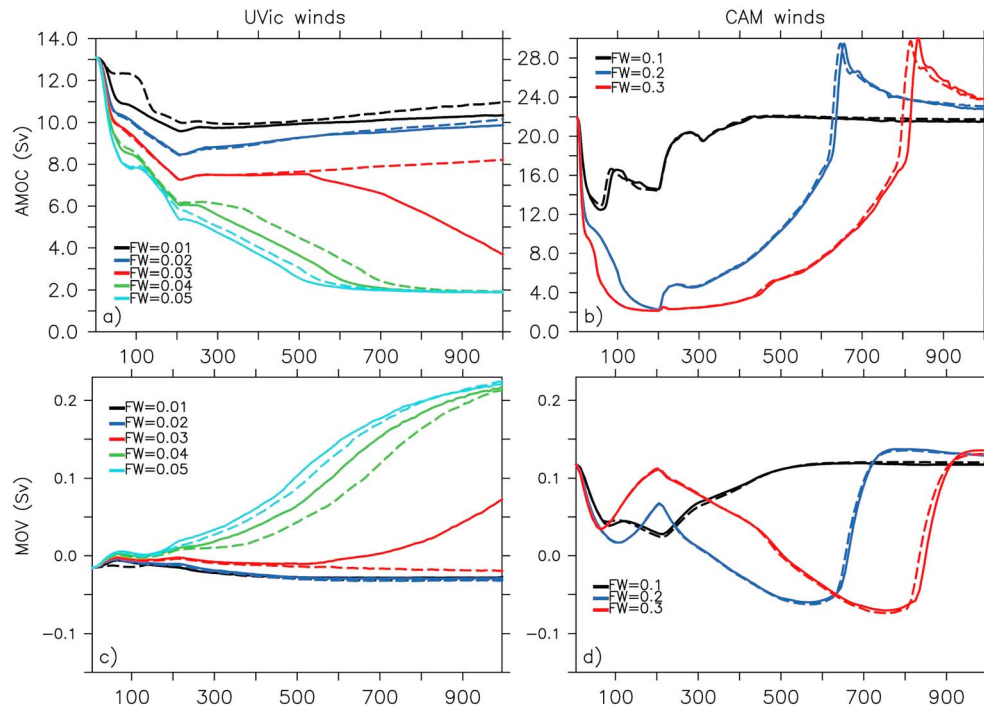
Figure 10. (a and b) AMOC strength and (c and d) Mov time series for the experiments with FW (dashed lines) and FW + H1 dust (solid lines) using (left) UVic-winds and (right) CAM-winds. The colors represent the different FW amounts added to the Ruddiman Belt (45° to 65°N).

3.3. Impact of Dust and Freshwater Forcing on AMOC

Next, we examine the combined impact of H1 dust and freshwater (FW) forcing during Heinrich stadials. Freshwater is imposed for 200 years and then turned off. Figures 10a and 10b show the AMOC time series under different FW forcing scenarios both with (solid lines) and without (dashed lines) H1 dust forcing. Both FW and H1 dust forcing result in a slowdown of the AMOC and a reversal in the north Atlantic OHT under both CAM and UVic-wind forcing (not shown), but differences arise when freshwater forcing is terminated. Under prescribed CAM-winds, the mean Mov term is positive (Figure 3b), and the AMOC is monostable. In this case the AMOC shuts down when the magnitude of hosing is FW = 0.2 Sv and FW = 0.3 Sv, but the AMOC recovers after FW ceases under all H1 + FW and FW only cases (Figure 10b). Under CAM-winds, with the exception of a short lag in the recovery, H1 dust does not significantly alter the time history of the AMOC (Figure 10b). This is consistent with the sign of the Mov term, which becomes negative (freshwater export) during the recovery period under the two larger FW forcing experiments (FW = 0.2 and 0.3 Sv), and transitions back to positive after the AMOC recovery near the end of the simulations (Figure 10d).

However, under prescribed UVic-winds, the Mov term is slightly negative (Figure 3a), AMOC is bistable, and thus the recovery depends on the magnitude of FW forcing (Figure 10a). Under UVic-winds, the two smaller freshwater forcing cases (FW = 0.01 and 0.02 Sv) result in a reduction in AMOC of 23 and 31%, respectively, and the AMOC gradually recovers after freshwater forcing ceases. In both cases, the simulation with H1 dust forcing causes a more abrupt AMOC reduction in the first 150 years (by ~1 Sv) and the recovery after FW ceases is slightly delayed. Under the largest freshwater forcing case (FW = 0.05 Sv), the AMOC shuts down to 2 Sv after 600 years and transitions to a stable off state. Thus, under prescribed UVic-winds, there is a threshold for AMOC collapse between 0.02 and 0.05 Sv, which is between 1×10^5 and 3×10^5 km^3 of cumulative FW at the end of 200 years. Under a more moderate amount of FW forcing (FW = 0.03 Sv), the system is closer to a threshold, and H1 dust leads to a bifurcation in the AMOC response (Figure 10a, red lines). This threshold is dependent on the duration of FW forcing. This same behavior, that dust triggers a bifurcation when the system is close to a threshold, is observed in additional sensitivity experiments with longer but weaker FW forcing (see the supporting information). As shown in the time series of MOV for the FW + H1 dust scenarios, the Mov term is negative in all simulations that show an AMOC recovery (Figure 10c). Mov becomes positive when the AMOC weakens in the largest FW cases (FW = 0.04 and 0.05 Sv) and in the case of
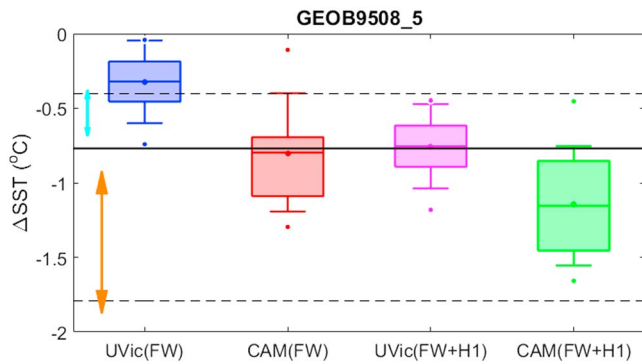
Figure 11. The black lines show the median HS1-LGM temperature anomaly (solid) and confidence interval (dashed; CI = 1st and 99th percentiles) at the GeoB9508-5 core. The temperature anomaly is calculated using the temperature over the HS1 interval (18–15 ka) minus the temperature over the LGM interval (21 ka + −2 ka). The arrows (dots) show the CI (median) of the individual alkenone (orange) and Mg/Ca (light blue) proxies. The box and whisker plots are the probability density functions (PDFs) based on the range of values of temperature difference between our FW experiments with and without H1 dust and the control LGM experiment. The boxes show the 25th to 75th percentiles with the median at the center; the whiskers give the 5th and 95th percentiles, and the dots give the 1st and 99th percentiles based on the derived PDFs.

FW = 0.03 Sv with H1 dust. Therefore, Mov acts as a positive feedback to the AMOC collapse in the UVic-wind scenarios, importing freshwater for a reduced AMOC.

3.4. Comparison to Proxy SST Records

Zarriess et al. (2011) analyzed Mg/Ca-based SST records from two cores in the eastern tropical Atlantic GeoB9508-5 at 15°N and GeoB9526-5 at 12°N off the northwestern coast of Africa and find that while earlier Heinrich stadials show opposing SST anomalies with cooling at the northern site and warming at the southern site, the most recent Heinrich stadials (HS1 and HS2) showed cooling in both locations. Figures S2 and S3 show the temperature anomalies with respect to the LGM averaged over the last century (years 900–1,000) in the UVic-wind experiments (Figure S2) and over model years 200–300 in the CAM-wind experiments (Figure S3), which is the period when the AMOC is weakest (Figures 10a and 10b). The bipolar see-saw response, with cooling in the North Atlantic and warming in the South Atlantic, is evident only in the larger FW forcing experiments when the largest reduction in AMOC occurs. Additionally, H1 dust forcing results in an additional cooling in the subtropical and tropical North Atlantic that shifts the anomalous warming further into the southern hemisphere, consistent with Zarriess et al. (2011).

We compare the recorded temperature change off the northwestern coast of Africa at gravity core GeoB9508-5 (Niedermeyer et al., 2009; Zarriess et al., 2011) to the temperature change in our FW and FW + H1 dust experiments with different prescribed wind fields (Figure 11). We utilize both the alkenone derived proxy record, which is obtained through alkenone paleothermometry and represents the yearly average of the mixed layer temperature (Niedermeyer et al., 2009), as well as the Mg/Ca based temperature reconstructions based on the planktic foraminiferal species *Globigerinoides ruber* (Zarriess et al., 2011). To derive the recorded temperature anomaly between HS1 and the LGM, we subtract the temperature records during HS1 (18–15 ka) from the temperature records during the LGM (21 ka ± 2 ka). The uncertainty in the proxy record is then calculated by bootstrapping these temperature difference values from each reconstruction separately and calculating their joint median value (solid black line) and confidence interval (CI = 1st and 99th percentiles) (dashed black lines). The median (CI) temperature anomaly (HS1-LGM) based on alkenones is −1.6 (−1.3, −2.0) °C, while the Mg/Ca-based temperature anomaly is much smaller at −0.53 (−.40, 0.64) °C (light orange and blue arrows, respectively). The temperature anomaly (H1-LGM) in our experiments is defined as difference in the temperature minima in all FW and FW + H1 dust experiments and the LGM control temperature. Probability density functions are calculated based on the five UVic-wind FW experiments, which range from 0.01 to 0.05 Sv, both with and without H1 dust, and the three CAM-wind FW experiments, which range from 0.1 to 0.3 Sv, both with and without H1 dust. Figure 11 shows the box and whisker plots for the UVic-wind FW + H1 dust, CAM-wind FW + H1 dust, UVic-wind FW, and CAM-wind FW experiments. Under FW forcing only, the UVic and CAM-wind experiments show a mean cooling of 0.3°C and 0.7°C, respectively. Although there is strong discrepancy between the two proxy data, the UVic FW distribution is mostly too weak and outside the paleoproxy range. Our UVic-wind FW + H1 dust experiments show a larger magnitude of cooling but still underestimate the cooling indicated by the alkenone-based SST anomaly. The CAM-wind experiments with both FW + H1 dust show cooling that is most comparable to mean of the joint proxy data (0.93°C), whereas only the CAM-wind FW + H1 distribution falls within the range from the alkenone-based SST anomaly.

We perform a similar analysis as shown in Figure 11 against two proxy records in the western and central North Atlantic (Figures S4 and S5). Sachs and Lehman (1999) analyzed sediments from the Bermuda Rise and found a 3 to 5° cooling (1 error bar = 0.17°C) associated with Heinrich stadials 4 and 5. Arienzo et al. (2015) used fluid inclusion analysis on a stalagmite from Abaco Island, Bahamas, and found an average 4.3 ± 2.7°C cooling for Heinrich stadials 1, 2, and 3. The degrees of cooling in our FW and FW + H1 dust simulations are well below these proxy records with less than 1°C cooling in the Bahamas and up to 2°C cooling at the Bermuda Rise. The amount of cooling again is largest in our FW + H1 dust simulation with CAM-wind forcing.

4. Discussion

Historically, freshwater forcing is viewed as the driver of the AMOC shut down during Heinrich events, and climate model simulations have shown a robust cooling of the North Atlantic and southward shift in the tropical rainbelt in response to FW input. Drying over North Africa is thought to drive the large increase in dust deposition in the eastern subtropical North Atlantic during these periods (Mulitza et al., 2008; McGee et al., 2013; Williams et al., 2016). However, there are large uncertainties in both the magnitude and duration of freshwater hosing during Heinrich events (Roche et al., 2014), and recently, Barker et al. (2015) questioned whether freshwater forcing was the driver or a consequence of North Atlantic cooling during Heinrich stadials. Additionally, modern observations show that atmospheric circulation changes (i.e., surface winds), and not precipitation changes, over North African dust source regions are the dominant driver of dust emissions (Evan et al., 2016). We hypothesized that enhanced Saharan dust can accelerate the climate changes associated with the Heinrich events. To test this hypothesis, we implemented a simple parameterization for the dust effects on shortwave and longwave radiations in UVic, using a Heinrich simulation performed with CCSM4. We tested the sensitivity of the dust-AMOC response to different amounts of dust loading in this intermediate complexity climate framework both with and without freshwater forcing. All of our simulations impose glacial boundary conditions, orbital parameters, and greenhouse gases forcing. Although the seasonality of the dust load is not implemented, and certain atmospheric feedbacks are not well represented in the simplistic one-layer atmospheric model of UVic, the E-P response to the additional dust loading is similar to the response found in a more sophisticated climate model with interactive dust forcing (CCSM4 in Murphy et al., 2014).

Wind stress forcing is prescribed in UVic and thus does not respond to the dust and FW forcings we impose. Since the strength of the glacial AMOC is not well constrained, we tested the impact of changing the prescribed wind field and implemented the dynamical wind feedback described in Weaver et al. (2001). We found that the strength of the AMOC under CAM-winds is much stronger (22 Sv) compared to the UVic-wind simulations (13 Sv). The strength of the AMOC may be tied to the rate of NADW formation and the strength of the Southern Ocean (SO) winds, both associated with a "pump" and "valve" system (Samelson, 2004), and they are linked to the AMOC stability in the adiabatic limit (e.g., Gnanadesikan & Toggweiler, 1999; Keeling, 2002; Nof et al., 2007). Indeed, increased SO winds under the CAM-wind forcing produce a monostable AMOC regime, whereas under the weaker UVic-wind forcing, a bistable regime is simulated. Observational studies suggest that the AMOC is bistable with stable "on" and "off" modes (Garzoli et al., 2012; Hofmann & Rahmstorf, 2009; Huisman et al., 2010; Liu et al., 2017), similar to our UVic-wind forcing experiments. In contrast, climate models typically show a monostable AMOC (Stouffer et al., 2006). A negative freshwater transport by the AMOC at the southern boundary indicates a net import of salt and a bistable AMOC regime, whereas a positive freshwater transport at the southern boundary indicates a AMOC regime with only one stable state (Hu et al., 2008; Weber et al., 2007; Weber & Drijfhout, 2007), similar to our CAM-wind forcing experiments.

Anomalous H1 dust forcing cools, extends sea ice coverage, and shifts the oceanic ventilation region southward in the North Atlantic. This is consistent with the theory that increased winter sea ice coverage can amplify Heinrich climate impacts (Broecker, 2006; Barker et al., 2015; Denton et al., 2005). Under UVic-wind forcing, although the time of triggering differs, all sensitivity experiments with different amounts of dust loading result in an abrupt reduction in AMOC by 20%, which is on the same order of the reduction predicted by climate change in year 2100 (Goes et al., 2010). This can be explained by the amount of freshwater added to the North Atlantic, which is related to the amount of dust loading. Initially, the cooler waters become trapped within the shallow subtropical cells and spread throughout the north and south Atlantic. Less evaporitic loss results in roughly 4 mSv of net freshwater convergence in the North Atlantic. This mechanism is less efficient in our simulations with prescribed CAM-winds where we find a <1 Sv reduction in AMOC after model year 500 (Figure 6b). The impact of changes in surface freshwater fluxes on AMOC has also been found to play a significant role on AMOC over the 20th century in CMIP5 models (Cheng et al., 2013). This suggests that additional dust loading over the North Atlantic can act as a potential trigger in slowing down the AMOC.

Including both freshwater and H1 dust results in a larger AMOC reduction that depends on the magnitude of FW forcing. Under small freshwater forcing H1 dust forcing initially causes a more abrupt decrease in the

AMOC, while under a more moderate amount of FW (FW = 0.03 Sv + H1 dust), the presence of H1 dust forcing can result in an AMOC collapse even after FW forcing ceases (under UVic-winds). Under CAM-wind forcing, H1 dust forcing does not significantly alter the AMOC response when FW forcing is applied. We performed additional sensitivity studies varying the duration and magnitude of FW forcing (supporting information). Even though dust did not contribute to AMOC changes in the CAM wind simulations, we do not discard that under longer or more progressive FW forcing dust can trigger bifurcations in the AMOC recovery, as suggested by those sensitivity experiments (Figure S6). Therefore, the interplay between the wind and hosing is crucial in determining the role of dust on triggering AMOC bifurcations.

We compare the magnitude of temperature change in our simulations to SST reconstructions in the North Atlantic. There is large uncertainty in the magnitude of cooling in the eastern subtropical Atlantic in the proxy data. In general, our CAM-wind simulations result in more cooling than the UVic-wind simulations throughout the North Atlantic. Including both FW + H1 dust forcing provides greater cooling in the eastern subtropical Atlantic, and the amount of cooling is within the range of proxy data. However, our simulations fail to reproduce the cooling estimated from Bahamian speleothems (Arienzo et al., 2015) and the Bermuda Rise marine sediment core (Sachs & Lehman, 1999), which suggests that we may be missing other important feedbacks, possibly clouds. Additionally, North American glacial dust sources (i.e., Peoria loess) may have provided an additional dust supply to the western North Atlantic during the glacial climate (Muhs et al., 2007) that we did not account for here.

5. Concluding Remarks

In conclusion, our results show that dust-climate feedbacks can provide an amplification to Heinrich cooling. Enhanced Saharan dust loading during H1 can extend the geographical range of cooling by locally influencing the radiative balance, increasing sea ice, and also through ocean dynamical feedbacks by destabilizing the AMOC. Anthropogenic warming is expected to increase meltwater discharge into the North Atlantic, which may have large implications on Sahel rainfall (Defrance et al., 2017). Our study suggests increased North African dust emissions, whether driven by AMOC changes or atmospheric circulation changes, could amplify the risk of an AMOC collapse. Therefore, it is important to include dust as an interactive component of the climate system.

References

Albani, S., Mahowald, N. M., Perry, A. T., Scanza, R. A., Zender, C. S., Heavens, N. G., … Otto-Bliesner, B. L. (2014). Improved dust representation in the Community Atmosphere Model. *Journal of Advances in Modeling Earth Systems*, 6(3), 541–570. https://doi.org/10.1002/2013MS000279

Arienzo, M. M., Swart, P. K., Pourand, A., Broad, K., Clement, A. C., Murphy, L. N., … Kakuk, B. (2015). Bahamian speleothem reveals temperature decrease associated with Heinrich stadials. *Earth and Planetary Science Letters*, 430, 377–386. https://doi.org/10.1016/j.epsl.2015.08.035

Baker, P. A., Rigsby, C. A., Seltzer, G. O., Fritz, S. C., Lowenstein, T. K., Bacher, N. P., & Veliz, C. (2001). Tropical climate changes at millennial and orbital timescales on the Bolivian Altiplano. *Nature*, 409(6821), 698–701. https://doi.org/10.1038/35055524

Bard, E., Rostek, F., Turon, J. L., & Gendreau, S. (2000). Hydrological impact of Heinrich events in the subtropical Northeast Atlantic. *Science*, 289(5483), 1321–1324. https://doi.org/10.1126/science.289.5483.1321

Barker, S., Chen, J., Gong, X., Jonkers, L., Knorr, G., & Thornalley, D. (2015). Icebergs not the trigger for North Atlantic cold events. *Nature*, 520(7547), 333–336. https://doi.org/10.1038/nature14330

Bitz, C. M., Holland, M. M., Weaver, A. J., & Eby, M. (2001). Simulating the ice-thickness distribution in a coupled climate model. *Journal of Geophysical Research*, 106(C2), 2441–2463. https://doi.org/10.1029/1999JC000113

Braconnot, P., Harrison, S. P., Otto-Bliesner, B., Abe-Ouchi, A., Jungclaus, J., & Peterschmitt, J.-Y. (2011). The Paleoclimate Modeling Intercomparison Project contribution to CMIP5. CLIVAR Exchanges No. 56 16, 15–19.

Brady, E. C., Otto-Bliesner, B. L., Kay, J. E., & Rosenbloom, N. (2013). Sensitivity to glacial forcing in the CCSM4. *Journal of Climate*, 26(6), 1901–1925. https://doi.org/10.1175/JCLI-D-11-00416.1

Broecker, W. S. (2006). Abrupt climate change revisited. *Global and Planetary Change*, 54(3–4), 211–215. https://doi.org/10.1016/j.gloplacha.2006.06.019

Bryan, F. (1986). High-latitude salinity effects and interhemispheric thermohaline circulations. *Nature*, 323(6086), 301–304. https://doi.org/10.1038/323301a0

Bryan, K., & Lewis, L. J. (1979). Water mass model of the World Ocean. *Journal of Geophysical Research*, 84(C5), 2503–2517. https://doi.org/10.1029/JC084iC05p02503

Calov, R., Ganopolski, A., Petoukhov, V., Claussen, M., & Greve, R. (2002). Large-scale instabilities of the Laurentide ice sheet simulated in a fully coupled climate system model. *Geophysical Research Letters*, 29(24), 2216. https://doi.org/10.1029/2002GL016078

Cheng, W., Chiang, J. C. H., & Zhang, D. (2013). Atlantic meridional overturning circulation (AMOC) in CMIP5 models: RCP and historical simulations. *Journal of Climate*, 26(18), 7187–7197. https://doi.org/10.1175/JCLI-D-12-00496.1

Clement, A. C., & Peterson, L. C. (2008). Mechanisms of abrupt climate change of the last glacial period. *Reviews of Geophysics*, 46, RG4002. https://doi.org/10.1029/2006RG000204

Cottet-Puinel, M., Weaver, A. J., Hillaire-Marcel, C., de Vernal, A., Clark, P. U., & Eby, M. (2004). Variation of Labrador Sea water formation over the last glacial cycle in a climate model of intermediate complexity. *Quaternary Science Reviews*, *23*(3–4), 449–465. https://doi.org/10.1016/S0277-3791(03)00123-9

De Vries, P., & Weber, S. L. (2005). The Atlantic freshwater budget as a diagnostic for the existence of a stable shut down of the meridional overturning circulation. *Geophysical Research Letters*, *32*, L09606. https://doi.org/10.1029/2004GL021450

Defrance, D., Ramstein, G., Charbit, S., Vrac, M., Famien, A. M., Sultan, B., … Vanderlinden, J. P. (2017). Consequences of rapid ice sheet melting on the Sahelian population vulnerability. *PNAS*, *114*(25), 6533–6538. https://doi.org/10.1073/pnas.1619358114

Denton, G. H., Alley, R. B., Comer, G. C., & Broecker, W. S. (2005). The role of seasonality in abrupt climate change. *Quaternary Science Reviews*, *24*(10-11), 1159–1182. https://doi.org/10.1016/j.quascirev.2004.12.002

Dickson, R. R., & Brown, J. (1994). The production of North Atlantic Deep Water—Sources, rates, and pathways. *Journal of Geophysical Research*, *99*(C6), 12,319–12,341. https://doi.org/10.1029/94JC00530

Dijkstra, H. A. (2007). Characterization of the multiple equilibria regime in a global ocean model. *Tellus*, *59A*, 695–705.

Drijfhout, S. S., Weber, S. L., & Swaluw, E. (2011). The stability of the MOC as diagnosed from model projections for pre-industrial, present and future climates. *Climate Dynamics*, *37*(7-8), 1575–1586. https://doi.org/10.1007/s00383-010-0930-z

Evan, A. T., Foltz, G. R., Zhang, D., & Vimont, D. J. (2011). Influence of African dust on ocean-atmosphere variability in the tropical Atlantic. *Nature Geoscience*, *4*(11), 762–765. https://doi.org/10.1038/ngeo1276

Evan, A. T., Flamant, C., Gaetani, M., & Guichard, F. (2016). The past, present and future of African dust. *Nature*, *531*(7595), 493–495. https://doi.org/10.1038/nature17149

Fanning, A. F., & Weaver, A. J. (1997). Temporal-geographical meltwater influences on the North Atlantic conveyor: Implications for the Younger Dryas. *Paleoceanography*, *12*(2), 307–320. https://doi.org/10.1029/96PA03726

Folland, C. K., Palmer, T. N., & Parker, D. E. (1986). Sahel rainfall and worldwide sea temperatures, 1901–85. *Nature*, *320*(6063), 602–607. https://doi.org/10.1038/320602a0

Fyke, J., & Eby, M. (2012). Comment on "Climate sensitivity estimated from temperature reconstructions of the Last Glacial Maximum". *Science*, *337*(6100), 1294. https://doi.org/10.1126/science.1221371

Garzoli, S. L., Baringer, M. O., Dong, S., Perez, R. C., & Yao, Q. (2012). South Atlantic meridional fluxes. *Deep Sea Research, Part I*, *71*, 21–32.

Gent, P. R., & Mcwilliams, J. C. (1990). Isopycnal mixing in ocean circulation models. *Journal of Physical Oceanography*, *20*(1), 150–155. https://doi.org/10.1175/1520-0485(1990)020%3C0150:IMIOCM%3E2.0.CO;2

Gnanadesikan, A., & Toggweiler, J. R. (1999). Constraints placed by silicon cycling on vertical exchange in general circulation models. *Geophysical Research Letters*, *26*(13), 1865–1868. https://doi.org/10.1029/1999GL900379

Goes, M., Urban, N. M., Tonkonojenkov, R., Haran, M., Schmittner, A., & Keller, K. (2010). What is the skill of ocean tracers in reducing uncertainties about ocean diapycnal mixing and projections of the Atlantic meridional overturning circulation? *Journal of Geophysical Research*, *115*, C12006. https://doi.org/10.1029/2010JC006407

Goes, M., Wainer, I., & Signorelli, N. (2014). Investigation of the causes of historical changes in the subsurface salinity minimum of the South Atlantic. *Journal of Geophysical Research: Oceans*, *119*, 5654–5675. https://doi.org/10.1002/2014JC009812

Hawkins, E., Smith, R. S., Allison, L. C., Gregory, J. M., Woollings, T. J., Pohlmann, H., & de Cuevas, B. (2011). Bistability of the Atlantic overturning circulation in a global climate model and links to ocean freshwater transport. *Geophysical Research Letters*, *38*, L10605. https://doi.org/10.1029/2011GL047208

Hofmann, H., & Rahmstorf, S. (2009). On the stability of the Atlantic meridional overturning circulation. *Proceedings of the National Academy of Sciences of the United States of America*, *106*(49), 20,584–20,589. https://doi.org/10.1073/pnas.0909146106

Hu, A., Otto-Bliesner, B. L., Meehl, G. A., Han, W., Morrill, C., Brady, E. C., & Briegleb, B. (2008). Response of thermohaline circulation to freshwater forcing under present-day and LGM conditions. *Journal of Climate*, *21*(10), 2239–2258. https://doi.org/10.1175/2007JCLI1985.1

Huisman, S. E., den Toom, M., & Dijkstra, H. A. (2010). An indicator of the multiple equilibria regime of the Atlantic meridional overturning circulation. *Journal of Physical Oceanography*, *40*(3), 551–567. https://doi.org/10.1175/2009JPO4215.1

Jullien, E., Grousset, F., Malaize, B., Duprat, J., Sanchez-Goni, M. F., Eynaud, F., … Flores, J. A. (2007). Low-latitude "dusty events" vs. high-latitude "icy Heinrich events". *Quaternary Research*, *68*(03), 379–386. https://doi.org/10.1016/j.yqres.2007.07.007

Kageyama, M., Paul, A., Roche, D. M., & Van Meerbeeck, C. J. (2010). Modelling glacial climatic millennial-scale variability related to changes in the Atlantic meridional overturning circulation: A review. *Quaternary Science Reviews*, *29*(21-22), 2931–2956. https://doi.org/10.1016/j.quascirev.2010.05.029

Kalnay, E., Kanamitsu, M., Kistler, R., Collins, W., Deaven, D., Gandin, L., … Joseph, D. (1996). The NCEP/NCAR 40-year reanalysis project. *Bulletin of the American Meteorological Society*, *77*(3), 437–471. https://doi.org/10.1175/1520-0477(1996)077%3C0437:TNYRP%3E2.0.CO;2

Keeling, R. F. (2002). On the freshwater forcing of the thermohaline circulation in the limit of low diapycnal diffusivity. *Journal of Geophysical Research*, *107*, C73077.

Labeyrie, L. D., Duplessy, J. C., Duprat, J., Juillet-Leclerc, A., Moyes, J., Michel, E., … Shackleton, N. J. (1992). Changes in the vertical structure of the North-Atlantic Ocean between glacial and modern times. *Quaternary Science Reviews*, *11*(4), 401–413. https://doi.org/10.1016/0277-3791(92)90022-Z

Lau, K. M., & Kim, K. M. (2007). Cooling of the Atlantic by Saharan dust. *Geophysical Research Letters*, *34*, L23811. https://doi.org/10.1029/2007GL031538

Liu, W., Xie, S.-P., Liu, Z., & Zhu, J. (2017). Overlooked possibility of a collapsed Atlantic meridional overturning circulation in warming climate. *Science Advances*, *3*(1), 1–7. https://doi.org/10.1126/sciadv.1601666

Malanotte-Rizzoli, P., Hedstrom, K., Arango, H., & Haidvogel, D. B. (2000). Water mass pathways between the subtropical and tropical ocean in a climatological simulation of the North Atlantic ocean circulation. *Dynamics of Atmospheres and Oceans*, *32*(3-4), 331–371. https://doi.org/10.1016/S0377-0265(00)00051-8

Manabe, S., & Stouffer, R. J. (1988). Two stable equilibria of a coupled ocean-atmosphere model. *Journal of Climate*, *1*(9), 841–866. https://doi.org/10.1175/1520-0442(1988)001%3C0841:TSEOAC%3E2.0.CO;2

Martinez Avellaneda, N., Serra, N., Minnett, P. J., & Stammer, D. (2010). Response of the eastern subtropical Atlantic SST to Saharan dust: A modeling and observational study. *Journal of Geophysical Research*, *115*, C08015. https://doi.org/10.1029/2009JC005692

McGee, D., deMenocal, P. B., Winckler, G., Stuut, J. B. W., & Bradtmiller, L. I. (2013). The magnitude, timing and abruptness of changes in North African dust deposition over the last 20,000 yr. *Earth and Planetary Science Letters*, *371*, 163–176.

McManus, J. F., Francois, R., Gherardi, J. M., Keigwin, L. D., & Brown-Leger, S. (2004). Collapse and rapid resumption of Atlantic meridional circulation linked to deglacial climate changes. *Nature*, *428*(6985), 834–837. https://doi.org/10.1038/nature02494

Muglia, J., & Schmittner, A. (2015). Glacial Atlantic overturning increased by wind stress in climate models. *Geophysical Research Letters*, *42*, 9862–9868. https://doi.org/10.1002/2015GL064583

Muhs, D. R., Budahn, J. R., Prospero, J. M., & Carey, S. N. (2007). Geochemical evidence for African dust inputs to soils of western Atlantic islands: Barbados, the Bahamas, and Florida. *Journal of Geophysical Research*, *112*, F02009. https://doi.org/10.1029/2005JF000445

Mulitza, S., Prange, M., Stuut, J.-B., Zabel, M., von Dobeneck, T., Itambi, A. C., … Wefer, G. (2008). Sahel megadroughts triggered by glacial slowdowns of Atlantic meridional overturning circulation. *Paleoceanography*, *23*, PA4206. https://doi.org/10.1029/2008PA001637

Murphy, L. N., Clement, A. C., Albani, S., Mahowald, N. M., Swart, P., & Arienzo, M. M. (2014). Simulated changes in atmospheric dust in response to a Heinrich stadial. *Paleoceanography*, *29*, 30–43. https://doi.org/10.1002/2013PA002550

Niedermeyer, E. M., Prange, M., Mulitza, S., Mollenhauer, G., Schefub, E., & Schulz, M. (2009). Extratropical forcing of Sahel aridity during Heinrich stadials. *Geophysical Research Letters*, *36*, L20707. https://doi.org/10.1029/2009GL039687

Nof, D., Van Gorder, S., & de Boer, A. (2007). Does the Atlantic meridional overturning cell really have more than one stable steady state? *Deep-Sea Research Part I*, *54*(11), 2005–2021. https://doi.org/10.1016/j.dsr.2007.08.006

Otto-Bliesner, B. L., & Brady, E. C. (2010). The sensitivity of the climate response to the magnitude and location of freshwater forcing: Last Glacial Maximum experiments. *Quaternary Science Reviews*, *29*(1-2), 56–73. https://doi.org/10.1016/j.quascirev.2009.07.004

Pacanowski, R. C. (1995). MOM 2 documentation: Users guide and reference manual, ver. 1.0, Ocean Group Tech. Rep. 3, Geophys. Fluid Dyn. Lab., Princeton, N. J.

Peterson, L. C., & Haug, G. H. (2006). Variability in the mean latitude of the Atlantic intertropical convergence zone as recorded by riverine input of sediments to the Cariaco Basin (Venezuela). *Palaeogeography Palaeoclimatology Palaeoecology*, *234*(1), 97–113. https://doi.org/10.1016/j.palaeo.2005.10.021

Peterson, L. C., Haug, G. H., Hughen, K. A., & Röhl, U. (2000). Rapid changes in the hydrologic cycle of the tropical Atlantic during the last glacial. *Science*, *290*(5498), 1947–1951. https://doi.org/10.1126/science.290.5498.1947

Rahmstorf, S. (1996). On the freshwater forcing and transport of the Atlantic thermohaline circulation. *Climate Dynamics*, *12*(12), 799–811. https://doi.org/10.1007/s003820050144

Rahmstorf, S., Crucifix, M., Ganopolski, A., Goosse, H., Kamenkovich, I. V., Knutti, R., … Weaver, A. J. (2005). Thermohaline circulation hysteresis: A model Intercomparison. *Geophysical Research Letters*, *32*, L23605. https://doi.org/10.1029/2005GL023655

Ridley, D. A., Heald, C. L., & Prospero, J. M. (2014). What controls the recent changes in African mineral dust aerosol across the Atlantic? *Atmospheric Chemistry and Physics*, *14*(11), 5735–5747. https://doi.org/10.5194/acp-14-5735-2014

Roche, D. M., Paillard, D., Caley, T., & Waelbroeck, C. (2014). LGM hosing approach to Heinrich event 1: Results and perspectives from data-model integration using water isotopes. *Quaternary Science Reviews*, *106*, 247–261. https://doi.org/10.1016/j.quascirev.2014.07.020

Ruddiman, W. F. (1977). Late Quaternary deposition of ice-rafted sand in subpolar North-Atlantic (lat 40-degrees to 65-degrees-N). *Geological Society of America Bulletin*, *88*(12), 1813–1827. https://doi.org/10.1130/0016-7606(1977)88%3C1813:LQDOIS%3E2.0.CO;2

Sachs, J., & Lehman, S. J. (1999). Subtropical North Atlantic temperatures 60,000 to 30,000 years ago. *Science*, *286*(5440), 756–759. https://doi.org/10.1126/science.286.5440.756

Samelson, R. M. (2004). Simple mechanistic models of middepth meridional overturning. *Journal of Physical Oceanography*, *34*(9), 2096–2103. https://doi.org/10.1175/1520-0485(2004)034%3C2096:SMMOMM%3E2.0.CO;2

Schefuß, E., Kuhlmann, H., Mollenhauer, G., Prange, M., & Pätzold, J. (2011). Forcing of wet phases in southeast Africa over the past 17,000 years. *Nature*, *480*(7378), 509–512. https://doi.org/10.1038/nature10685

Schefuß, E., Schouten, S., & Schneider, R. R. (2005). Climatic controls on central African hydrology during the last 20,000 years. *Nature*, *437*. 1003–1006. https://doi.org/10.1038/nature03945

Schmittner, A., Meissner, K. J., Eby, M., & Weaver, A. J. (2002). Forcing of the deep ocean circulation in simulations of the Last Glacial Maximum. *Paleoceanography*, *17*, 1015. https://doi.org/10.1029/2001PA000633

Schmittner, A., Urban, N. M., Shakun, J. D., Mahowald, N. M., Clark, P. U., Bartlein, P. J., … Rosell-Mele, A. (2011). Climate sensitivity estimated from temperature reconstructions of the Last Glacial Maximum. *Science*, *334*(6061), 1385–1388. https://doi.org/10.1126/science.1203513

Serra, N., Avellaneda, N. M., & Stammer, D. (2014). Large-scale impact of Saharan dust on the North Atlantic Ocean circulation. *Journal of Geophysical Research: Oceans*, *119*, 704–730. https://doi.org/10.1002/2013JC009274

Stager, J. C., Ryves, D. B., Chase, B. M., & Pausata, F. S. R. (2011). Catastrophic drought in the Afro-Asian monsoon region during Heinrich event 1. *Science*, *331*(6022), 1299–1302. https://doi.org/10.1126/science.1198322

Stocker, T. F., Timmerman, A., Renold, M., & Timm, O. (2007). Effects of salt compensation on the climate model response in simulations of large changes of the Atlantic meridional overturning circulation. *Journal of Climate*, *20*(24), 5912–5928. https://doi.org/10.1175/2007JCLI1662.1

Stommel, H. (1961). Thermohaline convection with two stable regimes of flow. *Tellus*, *13*, 224–230.

Stouffer, R. J., Yin, J., Gregory, J. M., Dixon, K. W., Spelman, M. J., Hurlin, W., … Weber, S. L. (2006). Investigating the causes of the response of the thermohaline circulation to past and future climate changes. *Journal of Climate*, *19*(8), 1365–1387. https://doi.org/10.1175/JCLI3689.1

Street-Perrott, F. A., & Perrott, R. A. (1990). Abrupt climate fluctuations in the tropics: The influence of Atlantic Ocean circulation. *Nature*, *343*(6259), 607–612. https://doi.org/10.1038/343607a0

Tjallingii, R., Claussen, M., Stuut, J.-B. W., Fohlmeister, J., Jahn, A., Bickert, T., … Roehl, U. (2008). Coherent high- and low-latitude control of the northwest African hydrological balance. *Nature Geoscience*, *1*(10), 670–675. https://doi.org/10.1038/ngeo289

Tréguier, A. M., Deshayes, J., Lique, C., Dussin, R., & Molines, J. M. (2012). Eddy contributions to the meridional transport of salt in the North Atlantic. *Journal of Geophysical Research*, *117*, C05010. https://doi.org/10.1029/2012JC007927

Valdivieso, M., Haines, K., Zuo, H., & Lea, D. (2014). Freshwater and heat transports from global ocean synthesis. *Journal of Geophysical Research: Oceans*, *119*, 394–409. https://doi.org/10.1002/2013JC009357

Vellinga, M., & Wu, P. (2008). Relations between northward ocean and atmosphere energy transports in a coupled climate model. *Journal of Climate*, *21*(3), 561–575. https://doi.org/10.1175/2007JCLI1754.1

Voelker, A. H. L., de Abreu, L., Schonfeld, J., Erlenkeuser, H., & Abrantes, F. (2009). Hydrographic conditions along the western Iberian margin during marine isotope stage 2. *Geochemistry, Geophysics, Geosystems*, *10*, Q12U08. https://doi.org/10.1029/2009GC002605

Wainer, I., Goes, M., Murphy, L. N., & Brady, E. (2012). Changes in the intermediate water mass formation rates in the global ocean for the Last Glacial Maximum, mid-Holocene and pre-industrial climates. *Paleoceanography*, *27*, PA3101. https://doi.org/10.1029/2012PA002290

Wang, X., Auler, A. S., Edwards, L., Cheng, H., Cristalli, P. S., Smart, P. L., … Shen, C.-C. (2004). Wet periods in northeastern Brazil over the past 210 kyr linked to distant climate anomalies. *Nature*, *432*(7018), 740–743. https://doi.org/10.1038/nature03067

Wang, X., Auler, A. S., Edwards, R. L., Cheng, H., Ito, E., & Solheid, M. (2006). Interhemispheric anti-phasing of rainfall during the last glacial period. *Quaternary Science Reviews*, *25*(23-24), 3391–3403. https://doi.org/10.1016/j.quascirev.2006.02.009

Wang, Y. J., Cheng, H., Edwards, R. L., An, Z. S., Wu, J. Y., Shen, C.-C., & Dorale, J. A. (2001). A high-resolution absolute-dated late pleistocene monsoon record from Hulu Cave, China. *Science*, *294*(5550), 2345–2348. https://doi.org/10.1126/science.1064618

Wang, C., Dong, S., Evan, A. T., Foltz, G. R., & Lee, S.-K. (2012). Multidecadal covariability of North Atlantic Sea surface temperature, African dust, Sahel rainfall, and Atlantic hurricanes. *Journal of Climate*, *25*(15), 5404–5415. https://doi.org/10.1175/JCLI-D-11-00413.1

Wang, W., Evan, A. T., Flamant, C., & Lavaysse, C. (2015). On the decadal scale correlation between African dust and Sahel rainfall: The role of Saharan heat low-forced winds. *Science Advances*, *1*(9), 1–5. https://doi.org/10.1126/sciadv.1500646

Weaver, A. J., Eby, M., Wiebe, E. C., Bitz, C. M., Duffy, P. B., Ewen, T. L., … Yoshimori, M. (2001). The UVic Earth System Climate Model: Model description, climatology, and applications to past, present and future climates. *Atmosphere-Ocean*, *39*(4), 361–428. https://doi.org/10.1080/07055900.2001.9649686

Weber, S. L., & Drijfhout, S. S. (2007). Stability of the Atlantic meridional overturning circulation in the Last Glacial Maximum climate. *Geophysical Research Letters*, *34*, L22706. https://doi.org/10.1029/2007GL031437

Weber, S. L., Drijfhout, S. S., Abe-Ouchi, A., Crucifix, M., Eby, M., Ganopolski, A., … Peltier, W. R. (2007). The modern and glacial overturning circulation in the Atlantic ocean in PMIP coupled model simulations. *Climate of the Past*, *3*(1), 51–64. https://doi.org/10.5194/cp-3-51-2007

Weijer, W., De Ruijter, W. P. M., Dijkstra, H. A., & van Leeuwen, P. J. (1999). Impact of interbasin exchange on Atlantic overturning. *Journal of Physical Oceanography*, *29*(9), 2266–2284. https://doi.org/10.1175/1520-0485(1999)029%3C2266:IOIEOT%3E2.0.CO;2

Williams, R., McGee, D., Kinsley, C. W., Ridley, D. A., Hu, S., Fedorov, A., … de Menocal, P. B. (2016). Glacial to Holocene changes in trans-Atlantic Saharan dust transport and dust-climate feedbacks. *Science Advances*, *2*(11), e1600445. https://doi.org/10.1126/sciadv.1600445

Wu, P., & Wood, R. (2008). Convection induced long term freshening of the subpolar North Atlantic Ocean. *Climate Dynamics*, *31*(7-8), 941–956. https://doi.org/10.1007/s00382-008-0370-1

Zarriess, M., Johnstone, H., Prange, M., Steph, S., Groeneveld, J., Mulitza, S., & Mackensen, A. (2011). Bipolar seesaw in the northeastern tropical Atlantic during Heinrich stadials. *Geophysical Research Letters*, *38*, L04706. https://doi.org/10.1029/2010GL046070

Zhang, R., & Delworth, T. L. (2005). Simulated tropical response to a substantial weakening of the Atlantic thermohaline circulation. *Journal of Climate*, *18*(12), 1853–1860. https://doi.org/10.1175/JCLI3460.1